

Imprints of the molecular-orbital geometry on the high-harmonic ellipticity

Meiyan Qin,¹ Xiaosong Zhu,¹ Kunlong Liu,¹ Qingbin Zhang,^{1,2,3} and Peixiang Lu^{1,2*}

¹Wuhan National Laboratory for Optoelectronics and School of Physics, Huazhong University of Science and Technology, Wuhan 430074, China

²MOE Key Laboratory of Fundamental Quantities Measurement, Wuhan 430074, China

³zhangqingbin@mail.hust.edu.cn

*lupeixiang@mail.hust.edu.cn

Abstract: The influence of the orbital symmetry on the ellipticity of the high-order harmonics is investigated. It is found that the ellipticity maps have distinct shapes for the molecular orbitals with different symmetry. Our analysis shows that the feature of the harmonic ellipticity map is essentially determined by the nodal structure of the nonsymmetric orbital. The results indicate that the molecular-orbital geometry is imprinted on the ellipticity of the high-order harmonics, which invites the use of ellipticity measurements as a probe of the orbital structure for polar molecules.

© 2022 Optical Society of America

OCIS codes: (190.7110) Ultrafast nonlinear optics; (190.4160) Multi-harmonic generation.

References and links

1. M. Lein, N. Hay, R. Velotta, J. P. Marangos, and P. L. Knight, "Role of the intramolecular phase in high-harmonic generation," *Phys. Rev. Lett.* **88**, 183903 (2002).
2. M. Lein, "Molecular imaging using recolliding electrons," *J. Phys. B: At. Mol. Opt. Phys.* **40**, R135-R173 (2007).
3. Q. Liao, Y. Zhou, C. Huang, and P. Lu, "Multiphoton rabi oscillations of correlated electrons in strong-field nonsequential double ionization," *New J. Phys.* **14**, 013001 (2012).
4. W. Hong, P. Lu, P. Lan, Q. Zhang, and X. Wang, "Few-cycle attosecond pulses with stabilized-carrier-envelope phase in the presence of a strong terahertz field," *Opt. Express* **17**, 5139-5146 (2009).
5. J. Itatani, J. Levesque, D. Zeidler, H. Niikura, H. Pépin, J. C. Kieffer, P. B. Corkum, and D. M. Villeneuve, "Tomographic imaging of molecular orbitals," *Nature* **432**, 867-871 (2004).
6. G. N. Gibson and J. Biegert, "Influence of orbital symmetry on high-order-harmonic generation and quantum tomography," *Phys. Rev. A* **78**, 033423 (2008).
7. E. V. Zwan, C. C. Chirilă, and M. Lein, "Molecular orbital tomography using short laser pulses," *Phys. Rev. A* **78**, 033410 (2008).
8. S. Haessler, J. Caillat, and P. Salières, "Self-probing of molecules with high harmonic generation," *J. Phys. B: At. Mol. Opt. Phys.* **44**, 203001-203041 (2011).
9. S. Ramakrishna, and T. Seideman, "Information content of high harmonics generated from aligned molecules," *Phys. Rev. Lett.* **99**, 113901 (2007).
10. Y. Mairesse, J. Higuët, N. Dudovich, D. Shafer, B. Fabre, E. Mével, E. Constant, S. Patchkovskii, Z. Walters, M. Yu. Ivanov, and O. Smirnova, "High harmonic spectroscopy of multichannel dynamics in strong-field ionization," *Phys. Rev. Lett.* **104**, 213601 (2010).
11. O. Smirnova, S. Patchkovskii, Y. Mairesse, N. Dudovich, D. Villeneuve, P. Corkum, and M. Yu. Ivanov, "Attosecond circular dichroism spectroscopy of polyatomic molecules," *Phys. Rev. Lett.* **102**, 063601 (2009).
12. E. Hijano, C. Serrat, G. N. Gibson, and J. Biegert, "Orbital geometry determined by orthogonal high-order harmonic polarization components," *Phys. Rev. A* **81**, 041401(R) (2010).
13. J. Levesque, Y. Mairesse, N. Dudovich, H. Pépin, J. C. Kieffer, P. B. Corkum, and D. M. Villeneuve, "Polarization state of high-order harmonic emission from aligned molecules," *Phys. Rev. Lett.* **99**, 243001 (2007).

14. X. Zhou, R. Lock, N. Wagner, W. Li, H. C. Kapteyn, and M. M. Murnane, "Elliptically polarized high-order harmonic emission from molecules in linearly polarized laser fields," *Phys. Rev. Lett.* **102**, 073902 (2009).
15. H. Niikura, N. Dudovich, D. Villeneuve, and P. Corkum, "Mapping molecular orbital symmetry on high-order harmonic generation spectrum using two-color laser fields," *Phys. Rev. Lett.* **105**, 053003 (2010).
16. J. Levesque, D. Zeidler, J. Marangos, P. Corkum, and D. Villeneuve, "High harmonic generation and the role of atomic orbital wave functions," *Phys. Rev. Lett.* **98**, 183903 (2009).
17. M. Qin, X. Zhu, Q. Zhang, W. Hong, and P. Lu, "Broadband large-ellipticity harmonic generation with polar molecules," *Opt. Express* **19**, 25084-25082 (2011).
18. C. Faria, and B. Augstein, "Molecular high-order harmonic generation with more than one active orbital: Quantum interference effects," *Phys. Rev. A* **81**, 043409 (2010).
19. B. Augstein, and C. Faria, "Influence of asymmetry and nodal structures on high-harmonic generation in heteronuclear molecules," *J. Phys. B: At. Mol. Opt. Phys* **44**, 055601-055611 (2011).
20. M. J. Frisch, G. W. Trucks, H. B. Schlegel, G. E. Scuseria, M. A. Robb, J. R. Cheeseman, J. A. Montgomery Jr., T. Vreven, K. N. Kudin, J. C. Burant, J. M. Millam, S. S. Iyengar, J. Tomasi, V. Barone, B. Mennucci, M. Cossi, G. Scalmani, N. Rega, G. A. Petersson, H. Nakatsuji, M. Hada, M. Ehara, K. Toyota, R. Fukuda, J. Hasegawa, M. Ishida, T. Nakajima, Y. Honda, O. Kitao, H. Nakai, M. Klene, X. Li, J. E. Knox, H. P. Hratchian, J. B. Cross, V. Bakken, C. Adamo, J. Jaramillo, R. Gomperts, R. E. Stratmann, O. Yazyev, A. J. Austin, R. Cammi, C. Pomelli, J. W. Ochterski, P. Y. Ayala, K. Morokuma, G. A. Voth, P. Salvador, J. J. Dannenberg, V. G. Zakrzewski, S. Dapprich, A. D. Daniels, M. C. Strain, O. Farkas, D. K. Malick, A. D. Rabuck, K. Raghavachari, J. B. Foresman, J. V. Ortiz, Q. Cui, A. G. Baboul, S. Clifford, J. Cioslowski, B. B. Stefanov, G. Liu, A. Liashenko, P. Piskorz, I. Komaromi, R. L. Martin, D. J. Fox, T. Keith, M. A. Al-Laham, C. Y. Peng, A. Nanayakkara, M. Challacombe, P. M. W. Gill, B. Johnson, W. Chen, M. W. Wong, C. Gonzalez, and J. A. Pople, *Gaussian 03, Revision C.02*, Gaussian Inc., Wallingford, CT (2010).
21. P. B. Corkum, "Plasma perspective on strong field multiphoton ionization," *Phys. Rev. Lett.* **71**, 1994-1997 (1993).
22. M. Lewenstein, Ph. Balcou, M. Yu. Ivanov, A. L'Huillier, and P. Corkum, "Theory of high-harmonic generation by low-frequency laser fields," *Phys. Rev. A* **49**, 2117-2132 (1994).
23. P. Lan, P. Lu, W. Cao, Y. Li, and X. Wang, "Isolated sub-100-as pulse generation via controlling electron dynamics," *Phys. Rev. A* **76**, 011402(R) (2007).
24. S. Son, D. A. Telnov, and S. Chu, "Probing the origin of elliptical high-order harmonic generation from aligned molecules in linearly polarized laser fields," *Phys. Rev. A* **82**, 043829 (2010).

1. Introduction

Progress in strong-field physics has made it possible to probe the molecular structure and dynamics with attosecond and Ångström resolutions [1–4]. High-order harmonic generation (HHG), which occurs in the interaction of strong field with atoms or molecules, is one of the most important tool for probing the molecular structure and dynamics. In particular, the application of HHG in the molecular orbital tomography (MOT) and attosecond probing of electronic dynamics in molecules has attracted a great deal of attention in the past decade [5–11]. Combined with molecular alignment techniques, the reconstruction of the highest occupied molecular orbital (HOMO) of N₂ was demonstrated in 2004 [5]. The studies of MOT have shown that the orbital symmetry plays an important role in the reconstruction of the molecular wavefunction [5–8]. Therefore, the prior knowledge of the orbital symmetry is essential to the molecular orbital tomography based on the HHG.

In previous works, several methods were proposed to probe the orbital symmetry [12–16]. For example, the information of the orbital symmetry can be decoded from the polarization angle of the high-order harmonics with respect to the driving linearly polarized laser field [12–14]. Another method to probe the orbital symmetry is to measure the alignment-dependent harmonic spectrum [15, 16]. In these works, the investigated molecular states are symmetric with defined parity (gerade or ungerade). Whereas for nonsymmetric orbitals that are neither gerade nor ungerade, obtaining the information about the orbital geometry has not been specifically discussed. In our recent work, it has been shown that for nonsymmetric molecular states, the ellipticity of the high harmonics are quite large in a wide spectral range, and this polarization property is mainly attributed to the nonsymmetric structure of the orbital [17]. Thus, it would be an effective method to obtain the information of the orbital geometry from the ellipticity of

the high-order harmonics for nonsymmetric molecular states.

In this paper, we investigate the influence of the orbital symmetry on the ellipticity of the high-order harmonics generated from nonsymmetric molecular states. It is found that the ellipticity maps of the high-order harmonics have unique shapes for orbitals with different symmetry. In order to gain a deeper insight into the features of the harmonic ellipticity, structural analysis of these molecular orbitals is performed. In addition, the individual contributions of s and p atomic states of the molecular orbital to the ellipticity of the high-order harmonics are also discussed.

2. Theoretical model

The molecular orbitals are simulated by using the linear combination of atomic orbitals (LCAO) approximation, along with the Born Oppenheimer approximation [18, 19]. Under these assumptions, the molecular orbital wavefunction is given by

$$\psi_0(\mathbf{r}) = \sum_n c_1^n \varphi_1^n(\mathbf{r} - \mathbf{R}_1) + c_2^n \varphi_2^n(\mathbf{r} - \mathbf{R}_2) \quad (1)$$

In this equation, the sum over n denotes the sum over the atomic orbitals. The number is used to distinguish the different molecular centers. The internuclear separation is given by $R = |\mathbf{R}_1 - \mathbf{R}_2|$. All these parameters are extracted from the Gaussian 03 ab initio code [20]. Gaussian-type orbitals with the 6-311G basis set are employed. The z-axis in the lab frame is defined as the polarization axis of the linearly polarized laser. The molecular axis is rotated in the y-z plane. The orientation angle between the internuclear axis and the z axis is denoted by θ . The driving laser field propagates along the x-axis.

A widely used quantum theory to model the process of the high harmonic generation is the strong field approximation (SFA) [21–23]. With its analytical and fully quantum-mechanical formulations for high harmonics, one can make a clear interpretation of the results in terms of classical physics. It has been shown that the expression for the HHG field can be factorized into two terms: the recombination dipole matrix element and a complex continuum electron wave packet (EWP) amplitude, when extremely short laser pulse is applied [7, 8, 16]. Accordingly, the HHG field of the components parallel and perpendicular to the polarization axis of the driving field are given by (in atomic units)

$$A_z(\omega, \theta) = 2\pi\omega W(E_k, \theta) d_z(k; \theta) \quad (2)$$

$$A_y(\omega, \theta) = 2\pi\omega W(E_k, \theta) d_y(k; \theta) \quad (3)$$

In these equations, ω is the frequency of the high harmonic emission, and $E_k = k^2/2$ is the kinetic energy of the returning electron. They are related through $\omega = E_k + I_p$, with I_p being the ionization energy of the state that the electron ionized from. $W(E_k, \theta)$ stands for the returning electron wave packet (EWP) amplitude. The complex wave packet in eq. (2) and eq. (3) are identical, since the returning electron is the same for the two components of the harmonic field. d_y, d_z are the \mathbf{y}, \mathbf{z} components of the recombination dipole moment respectively. The recombination dipole moment is expressed as,

$$\vec{d}(k, \theta) = \langle \psi_0(x, y, z; \theta) | \vec{r} | e^{ikz} \rangle \quad (4)$$

In this equation, $\psi_0(x, y, z; \theta)$ is the investigated molecular orbital wavefunction given by equation (1). Using Eqs. (2)-(4), one can obtain the amplitude ratio and the phase difference of the two components of the high harmonics by $r = |A_y/A_z| = |d_y/d_z|$ and $\delta = \arg[A_y] - \arg[A_z] =$

$\arg[d_y] - \arg[d_z]$. The ellipticity of the high-order harmonics ε as a function of r and δ is given by [24]:

$$\varepsilon = \sqrt{\frac{1+r^2 - \sqrt{1+2r^2 \cos 2\delta + r^4}}{1+r^2 + \sqrt{1+2r^2 \cos 2\delta + r^4}}} \quad (5)$$

The range of the ellipticity is $0 \leq \varepsilon \leq 1$. The linear, elliptical, and circular polarization correspond to $\varepsilon = 0$, $0 < \varepsilon < 1$, and $\varepsilon = 1$ respectively. When $r = 1$ and $\delta = \pi/2$, circularly polarized high-order harmonics with $\varepsilon = 1$ will be obtained.

3. Result and discussion

Four typical types of nonsymmetric orbitals are considered: π -type bonding and anti-bonding orbitals, and σ -type bonding and anti-bonding orbitals. These orbitals correspond to four basic orbital symmetries which are denoted by π , π^* , σ and σ^* , respectively. Our study mainly focuses on the influence of the orbital symmetry on the ellipticity of the high-order harmonics. Hence the model molecules with similar internuclear distances (NO and CO) are used. The π^* highest occupied molecular orbital (HOMO) of NO and the π HOMO-1 of CO are considered in our investigation. For comparison, the parameters $c_1^n, c_2^n, \mathbf{R}_1, \mathbf{R}_2$ of the HOMO-1 of CO and the HOMO of NO are also used to construct σ^* and σ orbital wavefunctions, respectively. The parameters c_1^n, c_2^n of the HOMO of NO and the HOMO-1 of CO are listed in Table 1. With Eqs. (2)–(5), the ellipticity of the high-order harmonics are obtained for these molecular states. The results are presented in the upper panels of Fig. 1. The horizontal axis stands for the orientation angle, and the vertical axis stands for the kinetic energy of the returning electron. The range of the kinetic energy is from 5eV to 40eV. The sectional views of the molecular orbitals are also presented in Fig. 1 (the lower panels). The orientation angle θ is 0° for π , σ and σ^* orbitals, and is 50° for π^* orbital. The nodal structures of molecular orbitals are depicted by the white dashed lines.

TABLE 1: The parameters c_1^n, c_2^n used in our simulation

	$c_{1/2}^{1s}$	$c_{1/2}^{2s}$	$c_{1/2}^{3s}$	$c_{1/2}^{2p_y}$	$c_{1/2}^{2p_z}$	$c_{1/2}^{3p_y}$	$c_{1/2}^{3p_z}$	$c_{1/2}^{4p_y}$
HOMO of CO	-0.151 0.013	0.134 -0.016	0.776 -0.094	\	-0.384 0.221	\	-0.174 0.241	\
HOMO-1 of CO	\	\	\	0.252 0.446	\	0.199 0.486	\	\
HOMO of NO	\	\	\	0.255 -0.234	\	0.413 -0.358	\	0.402 -0.402

As shown in Fig. 1, the ellipticity maps have distinct shapes for π , π^* , σ and σ^* orbitals. In Fig. 1(a) for the π orbital, large ellipticity of the high harmonics are observed at small angles. Moreover, the maxima of the ellipticity appear almost at the same orientation angle of 12° for the kinetic energies above 20eV, as indicated by the white arrow. In panel (b) for π^* orbital, the ellipticity map of the high-order harmonics is divided into two parts with similar shapes by the white dashed line at 50° . In each part, one peak of the ellipticity of the high harmonics is observed at the orientation angle close to 50° . In panel (c) for σ orbital, one peak of the ellipticity of the high-order harmonics appears at the orientation angle close to 0° . Interestingly, the shape of the ellipticity map in Fig. 1(c) is quite similar to the shape of the right part in Fig. 1(b). In the case of σ^* orbital, the maxima of the ellipticity of the high harmonics are observed at large orientation angles around 60° for all the kinetic energy higher than 20eV, as indicated by the arrow in Fig. 1(d).

For clarity, the ellipticity as a function of the orientation angle for three given kinetic energies are presented in Fig. 2 for π , π^* , σ and σ^* orbitals. The black arrows indicate the maxima of

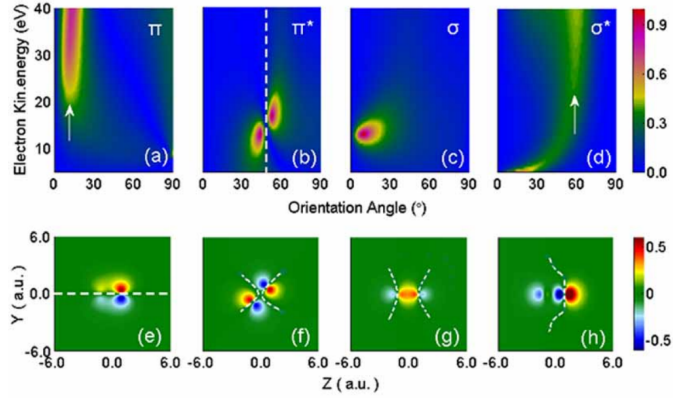


Fig. 1. The ellipticity maps for the π (panel a), π^* (panel b), σ (panel c) and σ^* (panel d) orbitals. The horizontal axis corresponds to the orientation angle, the vertical axis corresponds to the kinetic energy of the returning electron. In panels (a) and (d), the arrows indicate the maxima of the ellipticity for high kinetic energy (above 20eV). The sectional views of the corresponding molecular orbitals are presented in the second row. The orientation angle is 0° for the π , σ and σ^* orbitals, and is 50° for the π^* orbital. The nodal structures of molecular orbitals are depicted by the white dashed lines.

the ellipticity of the high harmonics. As shown in Fig. 2(a) for π orbital, large ellipticity of the high harmonics are obtained mainly at small orientation angles. The maxima of the ellipticity for high kinetic energy 24eV (the blue curves) and 35eV (the green curves) are almost fixed at a small orientation angle of 12° . While in panel (d) for σ^* orbital, these maxima appear around a large orientation angle of 60° . In panel (b) for π^* orbital, large ellipticity of the high harmonics are observed at intermediate angles. The ellipticity of the high-order harmonics at a given kinetic energy has two peaks around 50° . In panel (c) for σ , large ellipticity of the high harmonics are observed at small orientation angles close to 0° . The harmonic ellipticity at a given kinetic energy has one peak.

In Fig. 3, the harmonic spectra versus both the kinetic energy of the returning electron and the orientation angle are presented for the four molecular states. A three-cycle \sin^2 pulse with

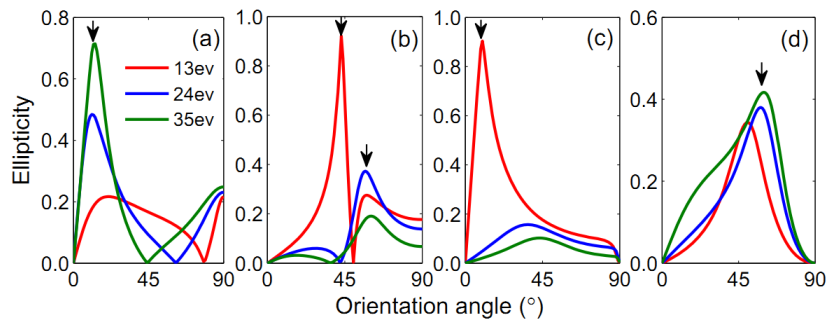


Fig. 2. The ellipticity as a function of the orientation angle for three given kinetic energies: 13eV (the red curve), 24eV (the blue curve), and 35eV (the green curve). Panels (a), (b), (c) and (d) correspond to the π , π^* , σ and σ^* orbitals, respectively. The black arrow indicates the maximum of the harmonic ellipticity.

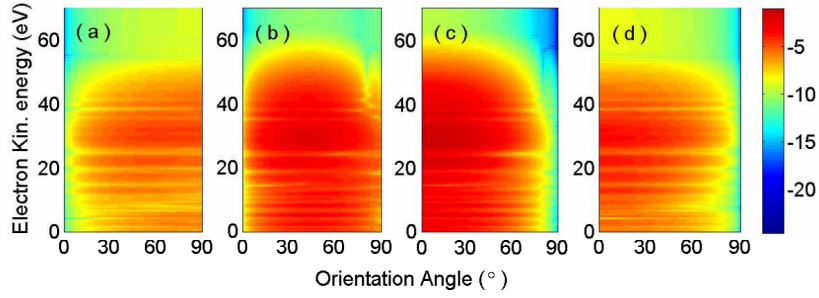


Fig. 3. The harmonic spectra for π (a), π^* (b), σ (c) and σ^* (d) orbitals. A three-cycle \sin^2 pulse with a carrier-envelope phase of 1.25π is used. The peak intensity and wavelength of the laser field are 2×10^{14} W/cm² and 800 nm, respectively. The horizontal axis corresponds to the orientation angle, and the vertical axis corresponds to the kinetic energy of the returning electron.

a carrier-envelope phase of 1.25π is used, where the factorization of the complex spectrum can be achieved [7]. The peak intensity and wavelength of the laser field are 2×10^{14} W/cm² and 800 nm, respectively. The high-order harmonics corresponding to the kinetic energy from 5eV to 40eV are well located in the plateau of the spectra for these molecular states. From Fig. 1 and Fig. 3, one can see that the ellipticity measurements considered in Fig. 1 correspond to measurable harmonic signals.

To gain a deeper insight into the features of the harmonic ellipticity observed in Figs. 1(a)–1(d), the structural analysis of the molecular state is performed. On the one hand, for the π and σ^* orbitals shown in Fig. 1(e) and Fig. 1(g), there is only one obvious nodal surface. In Fig. 1(e) for π orbital, the nodal surface is parallel to the z axis of the lab frame. Correspondingly, the maxima of the ellipticity for π orbital appear at small angles around 12° for all the kinetic energy above 20eV. In Fig. 1(h) for σ^* orbital, the nodal surface is perpendicular to the z axis of the lab frame disregarding the distortion of the nodal surface. Corresponding to this direction of the nodal surface, the maxima of the ellipticity of the high harmonics appear at large angles around 60° for all the kinetic energy higher than 20eV. Therefore, for the molecular state with only one obvious nodal plane, the maxima of the ellipticity of the high-order harmonics in high-energy range appear at almost the same orientation angle. This angle is determined by the direction of the nodal surface with respect to the z axis of the lab frame.

On the other hand, for the π^* and σ orbitals shown in Figs. 1(f)–1(g), there are two obvious nodal surfaces. In addition, the shape and direction of the nodal surfaces for π^* at the orientation angle of 50° are nearly the same as those of the nodal surfaces for σ at $\theta = 0^\circ$. As depicted by the white dashed lines, both the nodal surfaces show a “><” structure. Correspondingly, the peaks with similar shapes are observed in the right part ($\theta > 50^\circ$) of the ellipticity map for π^* and in the ellipticity map for σ . The location of the peak is close to 50° in the former case and close to 0° in the latter case. Additionally, in Fig. 1(f) for the π^* orbital, the orbital at $\theta = 50^\circ$ is approximately symmetric with respect to the z axis. The rotation of the nodal surfaces with θ varying from 50° to 0° is similar to that with θ from 50° to 90° . Thus the left part of the ellipticity map with θ varying from 50° to 0° has a similar shape to the right part with θ varying from 50° to 90° for π^* orbital. Both in the two parts, the peaks of the ellipticity of the high-order harmonics appear at the orientation angles close to 50° . It is shown that the nodal structures are imprinted on the ellipticity of the high-order harmonics and consequently the molecular orbitals with different symmetry correspond to distinct ellipticity maps.

To further confirm our conclusion, the ellipticity of the high-order harmonics for the molecular orbitals with various orbital distributions are investigated. These orbitals are constructed by the same atomic states as those in Fig. 1 with different weights of the contribution from the two nuclei. The nodal structures are the same as those in Fig. 1. The ellipticity maps of these molecular orbitals are presented in Fig. 4. From the first row to the third row, the weight of the contribution from nucleus 1 increases. Similar to those in Fig. 1, the results for the π and σ^* orbitals with only one nodal surface are presented in the first and last columns. As shown in Figs. 4(a)–4(c) for the π orbitals, large ellipticity of the high-order harmonics are observed at small angles, and the maxima of the ellipticity appear almost at the same orientation angle. The shapes of the ellipticity maps are similar to that in Fig. 1(a) and the location of the ellipticity maxima are also at around 12° . In the case of σ^* orbitals shown in the last column, the features of the harmonic ellipticity are also the same as that observed in Fig. 1(d), i.e. the maxima of the ellipticity of the high-order harmonics in high kinetic energy range locate around the large orientation angle of 60° . From Fig. 4(j) to Fig. 4(l), one can see that the ellipticity of the high-order harmonics decrease. This is because the orbital distribution tends to be symmetric when the weight of the contribution from nucleus 1 increases [17]. This phenomenon is also observed in the case of the π orbital when further increasing the weight of the contribution from nucleus 1.

The ellipticity maps of the high-order harmonics for the π^* and σ orbitals with the “><” nodal structure are presented in the second and third columns of Fig. 4. In the case of the π^* orbitals shown in Figs. 4(d)–4(f), all the ellipticity maps of the high-order harmonics are divided into two parts by the white dashed line at 50° . In each part, one peak of the ellipticity is observed at the orientation angle close to 50° . These features of the harmonic ellipticity are

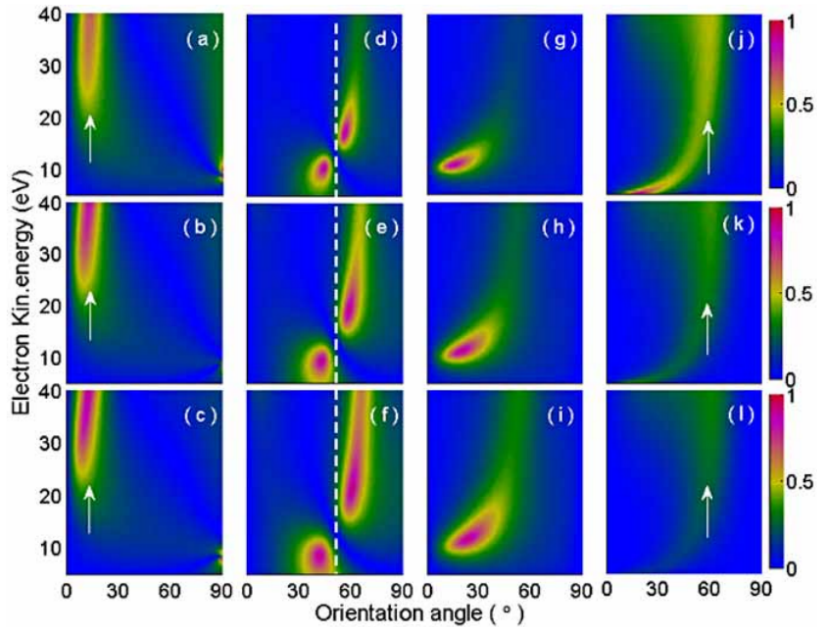


Fig. 4. The ellipticity maps of the high-order harmonics for the π (the first column), π^* (the second column), σ (the third column) and σ^* (the fourth column) orbitals with various weight of the contribution from nucleus 1 to the molecular orbital. From the first row to the third row, the weight of the contribution from nucleus 1 increases.

the same as those observed in Fig. 1(b). From Fig. 4(d) to Fig. 4(f), the shapes of the two parts of the ellipticity map become different. This is because the degree of asymmetry for the wavefunctions at 50° with respect to the z axis increases when the contribution of the atomic orbitals at nucleus 1 to the molecular orbitals increases. In the third column of Fig. 4 for the σ orbitals, one peak of the harmonic ellipticity is observed in each panel, which is consistent with that presented in Fig. 1(c). Therefore, in the four cases of the molecular orbitals with different symmetry, the main features of the harmonic ellipticity are not changed by varying the orbital distribution and are the same as those observed in Fig. 1.

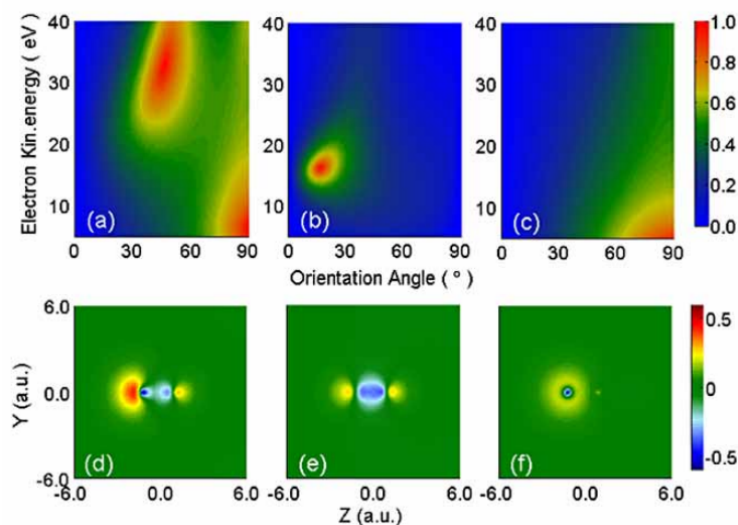


Fig. 5. The ellipticity map for (a) the full orbital of the CO HOMO, (b) the contribution from the p-type atomic states, (c) the contribution from the s-type atomic states. The sectional views of the corresponding wavefunctions are presented in lower panels. The orientation angle is 0° for all the wavefunctions.

The molecular orbitals considered in Fig. 1 are constructed from the p-type atomic states. According to the simulation with the Gaussian 03 ab initio code, the π and π^* orbitals are constructed entirely from p-type atomic states, while the σ and σ^* orbitals may be the mixing between s and p atomic states. Both the symmetry and nodal structure of the s atomic state are different from those of the p state. In the following, we employ the σ -type HOMO of CO to investigate the individual contributions of the s and p states to the ellipticity of the high-order harmonics. The parameters c_1^n, c_2^n of the HOMO of CO are given in Table 1. As in the references [18, 19], the parameters c_1^n, c_2^n of s (p) atomic states are set to zero when investigating the individual contributions of the p (s) atomic states. By comparing the ellipticity maps of the molecular orbitals with and without the contribution of s atomic states, we investigate the role played by the s-p mixing in the ellipticity of the high-order harmonics.

The ellipticity map of the high-order harmonics generated from the HOMO of CO is presented in Fig. 5(a). The individual contributions of the p and s states are displayed in Fig. 5(b) and Fig. 5(c), respectively. The sectional views of the corresponding wavefunctions are also presented in the lower panel. As shown in this panel, the HOMO of CO exhibits a strong mixing between s and p states. The nodal structure of the full σ orbital in Fig. 5(d) becomes a closed surface due to the mixing. The strong s p mixing will leave an imprint on the ellipticity of the high-order harmonics. In detail, the orbital wavefunction of the p states presented in Fig.

5(e) shows the same nodal structure (“><”) as that in Fig. 1(g). Correspondingly, the shape of the ellipticity map in Fig. 5(b) is similar to that in Fig. 1(c). In the case of the s atomic states shown in Fig. 5(c), the ellipticity map presents a new shape due to the new nodal structure and large ellipticity of the high-order harmonics are observed at the orientation angles around 90° . In Fig. 5(a) for the full σ orbital, large ellipticity of the high-order harmonics are obtained in two parts, due to the effect of the strong s-p mixing. The first part locates at large orientation angles around 90° and exhibits similar shape to that in Fig. 5(c) for the s states. The second part covers the orientation angles from 30° to 60° . Moreover, similar to the ellipticity map in Fig. 5(b) for the p states, there is also a peak in the second part. Accordingly, the harmonic ellipticity in the first part is mainly contributed by the s states, and the contribution of the p states dominates in the second part. To confirm this, we also study the harmonic ellipticity for the molecular orbitals with different weight of the contribution of the s states. It is found that large ellipticity observed at the orientation angles around 90° decreases quickly when the weight of the s states is reduced. The shape of the ellipticity map in Fig. 5(a) is changed into that presented in Fig. 5(b) when the weight of the s states is reduced to zero.

As shown in Fig. 1 and Fig. 5, the shapes of the ellipticity maps for the σ orbital (both with and without the s-p mixing) are distinct to those of the ellipticity maps for the π , π^* and σ^* orbitals. We also investigate the effect of the s-p mixing on the ellipticity of the high-order harmonics for the σ^* orbital. In general, the nodal structure of the σ^* orbital is not significantly changed by the s-p mixing due to the antibonding symmetry. Thus for the σ^* orbital (both with and without the s-p mixing), the ellipticity map of the high-order harmonics has similar shape to that presented in Fig. 1(d). The results indicate that one can obtain the information of the orbital symmetry from the ellipticity map of the high-order harmonics for the nonsymmetric orbitals.

As discussed in Section 2, extremely short laser pulse is required to achieve the factorization of the complex spectrum for nonsymmetric orbitals, which benefits the application of the harmonic ellipticity as a probe of the orbital structure. To further investigate the role played by the pulse duration, we also calculate the harmonic ellipticity map using the laser pulses with 10fs and 20fs duration, where the complex spectrum can not be factorized in the recombination dipole moment and a complex continuum EWP. It is found that the main features of the ellipticity maps for π , π^* , σ and σ^* orbitals remain the same as in Fig. 1. Therefore, the harmonic ellipticity as a probe of the orbital structure for the nonsymmetric orbitals is also applicable to the multi-cycle laser pulses.

4. Conclusion

We investigate the influence of the orbital symmetry on the ellipticity of the high harmonics for the nonsymmetric molecular states. It is found that the ellipticity maps of the high-order harmonics have distinct shapes for the molecular orbitals with different symmetry. To gain a deeper insight into the features of the high-harmonic ellipticity, the structural analysis is performed for the molecular orbitals. The nodal structure of the molecular orbital is found to be imprinted on the high-harmonic ellipticity and the feature of the high-harmonic ellipticity is essentially determined by the nodal structure of the molecular orbital. We also investigate the individual contributions of s and p atomic states to the ellipticity of the high-order harmonics for the σ and σ^* orbital. The results indicate that the ellipticity of the high-order harmonics can be used as a probe of the orbital structure for polar molecules

Acknowledgment

This work was supported by the National Natural Science Foundation of China under Grants No. 60925021, 10904045, 11104092 and the Doctoral fund of Ministry of Education of China

under Grant No. 20100142110047.